Remote Sens. **2015**, *7*, 7914-7937; doi:10.3390/rs70607914

OPEN ACCESS

remote sensing

ISSN 2072-4292

www.mdpi.com/journal/remotesensing

Article

Retrieval of High-Resolution Atmospheric Particulate Matter Concentrations from Satellite-Based Aerosol Optical Thickness over the Pearl River Delta Area, China

Lili Li [1,2], Jingxue Yang [3] and Yunpeng Wang [1,*]

[1] State Key Laboratory of Organic Geochemistry, Guangzhou Institute of Geochemistry, Chinese Academy of Sciences, Guangzhou 510640, China; E-Mail: lilili@gig.ac.cn

[2] University of Chinese Academy of Sciences, Beijing 100049, China

[3] Guangdong Research Institute of Water Resources and Hydropower, Guangzhou 510365, China; E-Mail: yang_jingxue@126.com

* Author to whom correspondence should be addressed; E-Mail: wangyp@gig.ac.cn; Tel./Fax: +86-20-852-901-97.

Academic Editors: Alexander Kokhanovsky and Prasad S. Thenkabail

Received: 30 January 2015 / Accepted: 10 June 2015 / Published: 17 June 2015

Abstract: Satellite remote sensing offers an effective approach to estimate indicators of air quality on a large scale. It is critically significant for air quality monitoring in areas experiencing rapid urbanization and consequently severe air pollution, like the Pearl River Delta (PRD) in China. This paper starts with examining ground observations of particulate matter (PM) and the relationship between PM_{10} (particles smaller than 10 μm) and aerosol optical thickness (AOT) by analyzing observations on the sampling sites in the PRD. A linear regression ($R^2 = 0.51$) is carried out using MODIS-derived 500 m-resolution AOT and PM_{10} concentration from monitoring stations. Data of atmospheric boundary layer (ABL) height and relative humidity are used to make vertical and humidity corrections on AOT. Results after correction show higher correlations ($R^2 = 0.55$) between extinction coefficient and PM_{10}. However, coarse spatial resolution of meteorological data affects the smoothness of retrieved maps, which suggests high-resolution and accurate meteorological data are critical to increase retrieval accuracy of PM. Finally, the model provides the spatial distribution maps of instantaneous and yearly average PM_{10} over the PRD. It is proved that observed PM_{10} is more relevant to yearly mean AOT than instantaneous values.

Keywords: aerosol optical thickness (AOT); particulate matter (PM); MODIS; vertical and humidity correction; Pearl River Delta

1. Introduction

Particulate matters (PM), or aerosols, not only have direct and indirect radiative forcing effects on climate systems [1,2], but also reduce visibility and induce respiratory diseases thus affecting air quality and human health [3]. The strong and consistent links between ambient PM exposure and adverse health effects have been shown in epidemiological and toxicological studies around the world [4–7]. Therefore, monitoring air quality at high spatial-temporal resolution is of great significance, especially for rapidly growing megacities which are facing severe air pollution owing to industrial development and population expansion.

Current ground measurement networks, though well-calibrated, are spatially-limited and inadequate to evaluate time-space dynamics of air pollution and effects on human health. Advances in satellite remote sensing have provided a cost-effective approach to frequently monitor the spatial distribution and the regional transport of aerosol particles on a large scale [8–14], though the discontinuous satellite observations could hardly reflect the diurnal variations of particle matters. Aerosol optical thickness (AOT), derived from satellite observations, is a dimensionless measure of aerosol abundance and atmospheric extinction of radiance over the entire air column. Previous researches have revealed a strong positive relationship between satellite-based measurements of AOT and ground-based measurements of particulate matters smaller than 2.5 μm and 10 μm in aerodynamic diameters ($PM_{2.5}$ and PM_{10}, respectively) [15–25]. A summary of linear AOT/PM relationships, intercepts and correlation coefficients in several previous studies is shown in Table 1. IDEA (Infusion satellite Data into Environmental air quality application), as a NASA-EPA-NOAA partnership, has produced the daily surface PM estimation across the United States from MODIS AOT products through predefined regression relation. Its time ranges from 1 January 2008 to the present, with a coarse spatial resolution of 10 km.

Located in south-central Guangdong, China (about 21.5°N–24°N and 112°E–115.5°E), the Pearl River Delta (PRD) (Figure 1) is an area that boasts the fastest economic growth and population increase in the world. It also has become an area of China which is facing the severest air pollution because of rapid industrial development, vegetation reduction, and heavy traffic pressure. Deaths and health effects resulting from air pollution in the PRD had been calculated from an economic perspective by scholars at Peking University. Economic losses caused by air pollution were estimated to be 292 billion RMB in 2006, accounting for 1.35% of the regional Gross Domestic Product (GDP) [26]. As a consequence, the increase in hazy days and deteriorating air quality, greatly impairing the health of the population and the visibility over the region, has drawn widespread attention from the Chinese government and the public [27–30]. However, there is still a lack of AOT-based estimations for PM concentrations in this area currently. By combining ground measurements and remote sensing observations, estimations of AOT-based PM concentrations, especially with high spatial resolution data, could offer spatially continuous mapping with high accuracy, which is useful for regional air quality monitoring.

Table 1. Literature survey linear AOT-PM relationships, intercepts and correlation coefficients.

Author	Study Area	Date	Model description	Linear Regression	R^2
Wang *et al.* [17]	Alabama	2002	MODIS 10 km AOT and $PM_{2.5}$	$77\tau - 0.23$ (Terra) $68.6\tau + 1.93$ (Aqua)	0.67 0.76
Chu *et al.* [18]	Italy	August–October 2000	AOT from AERONET and PM_{10}	$54.7\tau + 8$	0.82
Engel-cox *et al.* [11]	Eastern United States	Summer 2004	MODIS 10 km AOT and $PM_{2.5}$	$25.329\tau + 11.091$	0.574
Gupta *et al.* [20]	Global urban areas	2002	MODIS 10 km AOT and $PM_{2.5}$	$166.7\tau - 25$	0.96
Li *et al.* [21]	Hong Kong	15–17 September 2001	MODIS 1 km AOT and $PM_{2.5}$	$171.3\tau + 0.4$	0.77
Zheng *et al.* [22]	Pearl River Delta	2006 to 2008	MODIS 1 km AOT and PM_{10}	$63.35\tau + 39.94$	0.458
Guo *et al.* [23]	Eastern China	2007	MODIS 10 km AOT and hourly PM	NA	0.46 (PM_1) 0.61 ($PM_{2.5}$) 0.52 (PM_{10})
Schaap *et al.* [14]	Cabauw, Netherlands	August 2006 to May 2007	MODIS 10 km AOT and $PM_{2.5}$	$120\tau+5.0926$	0.518
Wang *et al.* [24]	Beijing	July 2007 to October 2008	MODIS 1 km AOT and PM_{10}	$361.1\tau + 19.6$	0.65
You *et al.* [25]	Xi'an	2013	MODIS 10 km AOT, MISR 17.6 km AOT and $PM_{2.5}$	NA	0.816 0.847

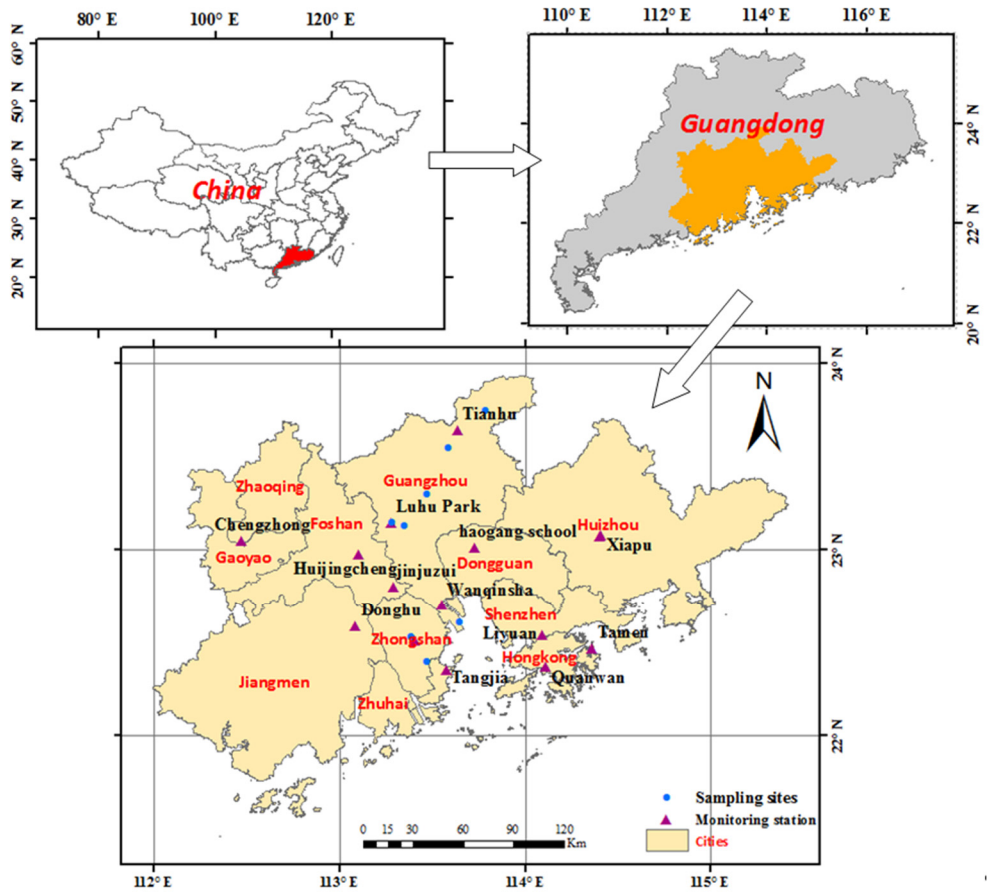

Figure 1. Location of 11 cities and the 15 air quality monitoring stations in the Pearl River Delta region in Guangdong Province, China. The blue spots in the map represent the sampling sites selected to conduct our ground observations of PM and AOT.

In this study, we developed correlative linear models between AOT and PM_{10} in the Pearl River Delta region, based upon ground-based observations from 2010 to 2011. We also explored the potential of retrieving the spatial distribution of particulate matters both daily and yearly from MODIS-derived AOT using these models, with an aim to provide more intuitive and reliable images of air quality in the area and reasonably illustrate the usefulness of satellite-derived AOT as a proxy for particulate matters.

2. Data

2.1. Station Monitoring Data of PM_{10}

Hourly air quality measurements from 15 monitoring stations Figure 1 from January 2008 to December 2008 were provided by the Department of Environmental Protection of Guangdong Province, China. Locations and the underlying surface types of the stations are shown in Table 2 and quoted from a report of monitoring results in 2008: Pearl River Delta regional air quality monitoring network. The measurements included concentrations of PM_{10} and major gaseous pollutants such as surface-level O_3, SO_2 and NO_2. Also, the government has fully implemented the QA/QC program to ensure that the air quality data from the monitoring stations are highly accurate and reliable, and the control limit set for PM_{10} are ±10%. Nevertheless, the sparse distribution of stations cannot reliably reflect the spatial distribution of atmospheric particulate matter over the Pearl River Delta region.

Table 2. Locations and types of the monitoring stations in the Pearl River Delta.

Stations	Type	(Lat, Lon)	City
Tianhu	Rural	(23.646° N, 113.638° E)	Guangzhou
Luhu Park	City	(23.156° N, 113.277° E)	Guangzhou
Haogang school	Mixed residential/commercial/industrial	(23.017° N, 113.734° E)	Dongguan
Xiapu	Urban: commercial	(23.054° N, 114.41° E)	Huizhou
Jinguowan	Residential	(23.074° N, 114.406° E)	Huizhou
Liyuan	City	(22.545° N, 114.089° E)	Shenzhen
Tamen	Rural	(22.477° N, 114.361° E)	Hong Kong
Quanwan	Mixed residential/commercial/industrial	(22.375° N, 114.115° E)	Hong Kong
Tangjia	Mixed educational/commercial and residential/commercial	(22.354° N, 113.58° E)	Zhuhai
Zimaling Park	Mixed residential/commercial	(22.509° N, 113.406° E)	Zhongshan
Wanqinsha	Mixed educational/commercial and residential/industrial	(22.709° N, 113.55° E)	Guangzhou
Donghu	City	(22.59° N, 113.087° E)	Jiangmen
Jinjuzui	Tourist and cultural/educational	(22.804° N, 113.291° E)	Foshan
Huijingcheng	Mixed residential/commercial/industrial	(22.978° N, 113.106° E)	Foshan
Chengzhong	Mixed residential/commercial	(23.053° N, 112.476° E)	Zhaoqing

2.2. Ground-Based Sampling Observations of AOT and PM

AOT ground observations were obtained using a MICROTOP II sun photometer Manufactured by U.S Solarlight Company. The MICROTOP II is a hand-held sun photometer for measuring aerosol optical thickness and direct solar irradiance at the following five discrete wavelengths: 380 nm, 500 nm, 870 nm, 936 nm and 1020 nm. The water vapor column can also be measured at the following

three wavelengths: 870 nm, 936 nm and 1020 nm. Features of MICROTOP II include high accuracy, ease of use, portability and instantaneous results.

A DustTrak DRX aerosol particulate monitor was used to measure the particulate concentrations in a wide variety of environments. It provided reliable exposure assessment by simultaneously measuring size-segregated mass fraction concentrations corresponding to PM_1, $PM_{2.5}$, PM_{10} and Total PM size fractions. The one-minute resolution of DustTrak DRX offers us an insight into the occurrence of high concentrations of PM, and the clear duration of the dust plumes. The comparison among eight PM_{10} measurement instruments shows that multiple size ranges in the DustTrak DRX could identify the spatial non-uniformity for the sources [31].

For the limitation of monitoring devices and manpower, we chose several sampling sites, including urban areas, suburbs and their borders in the three cities of the Pearl River Delta, to avoid the uncertainty caused by observations on a single underlying surface Table 3. The total number of sample points is 305, with 162 points in the urban areas and 143 points in the suburbs. Rapid urbanization process makes the difference between the locations less apparent, thus the monitoring results reflect the air quality of urban actually. The sampling time was from 10:30 a.m. to 3:00 p.m. between October 2010 and November 2011, to be consistent with the pass time of MODIS, about 11 a.m. for Terra and 2 p.m. for Aqua.

Table 3. Location of AOT and PM sampling sites in the Pearl River Delta.

Places	Type	Latitude(° N)	Longitude(° E)	N
Guangzhou Institute of Geochemistry	Urban	23.133	113.350	28
Guangzhou Luhu park	Borders of urban and suburb	23.15	113.283	66
Maofeng Mountain Forestry Park	Suburb	23.3	113.467	4
Conghua city	Urban	23.55	113.583	60
Liuxihe National Forest Park	Suburb	23.75	113.783	104
Zhongshan forest	Suburb	22.4	113.467	21
Zhongshan college	Urban	22.533	113.383	8
Nansha wetland park	Suburb by the sea	22.617	113.650	14

Notes: N is the number of sampling dataset.

2.3. Satellite Data

Data used in this study over the PRD from a Moderate-resolution imaging spectroradiometer (MODIS) (onboard the Terra and Aqua satellite) were downloaded from NASA LAADS (Level 1 and Atmosphere Archive and Distribution System). They are calibrated L1B data with 500 m spatial resolution including visible, near-infrared, and mid-infrared bands. The complete set of cloud-free remote sensing images during 2008 was acquired, together with monitoring data of air quality from 15 stations in 2008 provided by the Department of Environmental Protection of Guangdong Province, China.

2.4. Atmospheric Boundary Layer (ABL) Height and Relative Humidity (RH)

The National Centers for Environmental Prediction (NCEP) Climate Forest System Reanalysis (CFSR) provide global atmospheric analyzed products, such as boundary layer height and relative humidity, with a 0.5 degree horizontal resolution at 6-hourly intervals, initialized four times per day (0:00, 6:00, 12:00 and 18:00 UTC) [32] The products are proved to be accurate by using the 5-day

forecast scores as a measure of the accuracy of initial states [33]. We used data from 2, 3 and 5 January 2008 to perform height and humidity corrections on AOT.

3. Analyses on Particulate Concentration in the PRD

3.1. Ground Observations of Particulate Matter

The concentrations of PM_{10}, $PM_{2.5}$ and PM_1 are expressed in terms of milliequivalents of particles smaller than 10 μm, 2.5 μm and 1 μm in diameter per cubic meter of air in units of $\mu g/m^3$. Ground-based observations of PM_{10}, $PM_{2.5}$ and PM_1 at all the sampling sites from November 2010 to November 2011 were used to analyze the size distribution of particles. The percentage of PM_1 from $PM_{2.5}$ and PM_{10} calculated from all the sample points range from 90% to 100% and from 60% to 90%, respectively. Most of the atmospheric particles over the sampling sites are small-size respirable particles, consistent with research results by Wu [27,34,35]. He pointed out that the ratio of $PM_{2.5}$ to PM_{10} over PRD has obviously increased in the past two decades, reaching 60% to 80%, which is higher in dry seasons than in rainy seasons. Our results are slightly higher, perhaps caused by the difference between measuring instruments. The aerosol monitor used in our study is a continuous real-time 90° light-scattering laser photometer. Aerosol particles are absorbed into the optics chamber through the built-in air pump, and the concentration of the particles is measured by the amount of light scattering. The measurements of fine-mode particles are less accurate than those from β-ray decay method and tapered element oscillating microbalance (TEOM) method.

3.2. Station Monitoring Data of Particulate Matters in PRD

Measurements of PM_{10} from the 15 stations in the PRD at 11 a.m. (the passing time of Terra satellite) from 1 to 5 January are listed in Table 4. The PM_{10} concentration on most of the sites on 2 January increased especially at stations in Nansha (Guangzhou) and Foshan compared with those on 1 January. Dongguan, Foshan and Nansha became areas with peak value on 3 January and the value from Huijingcheng in Foshan was the highest, followed by Donghu in Jiangmen, Haogang School in Dongguan and Chenzhong in Zhaoqing on 4 January. In general, station measurements in Guangzhou, Conghua, Huizhou, Shenzhen and Hongkong did not change much during the period. Our field survey reveals that stations with small variations are mostly located in areas with high vegetation cover. This apparently enhances subsidence of atmospheric particles.

The hourly PM_{10} limit concentration in the Pearl River Delta is set to be 150 $\mu g/m^3$, according to the ambient air quality standards issued by China's Ministry of Environmental Protection and China's General Administration of Quality Supervision in 2012. Inspection of Table 4 shows that on 1 and 2 January PM_{10} of all sites were below this standard. However, on days of severe air pollution such as 3, 4 and 5 January, measurements were far above the standard threshold 150 $\mu g/m^3$ at Jinjuzui and Huijincheng in Foshan, Haogang school in Dongguan, Donghu in Jiangmen and Wanqinsha in Guangzhou. Concentrations of PM_{10} from several stations, exceeding the standard (150 $\mu g/m^3$), are marked in bold format.

Table 4. Station measurements of PM_{10} at 11:00 a.m. on 1–5 January 2008 ($\mu g/m^3$).

Stations	1 January	2 January	3 January	4 January	5 January
Tianhu	40	43	54	110	104
Luhu Park	31	27	34	39	79
Haogang school	48	73	**152**	**174**	**200**
Xiapu	101	122	133	147	**186**
Jinguowan	28	40	53	58	54
Liyuan	68	95	122	88	120
Tamen	--	89	92	64	111
Quanwan	--	64	91	52	101
Tangjia	33	34	77	61	79
Zimaling Park	52	67	119	79	**233**
Wanqinsha	88	125	**151**	23	**232**
Donghu	54	73	118	**197**	**336**
Jinjuzui	60	62	91	63	**190**
Huijingcheng	--	119	**197**	**265**	**311**
Chengzhong	62	78	119	**157**	146

3.3. Correlation Test between Particulate Concentration and AOT

We developed linear relationships between PM_{10} and aerosol optical thickness (AOT) at 500 nm by using 305 datasets of ground-based observation from our instruments between 18 October and 29 November 2011 (Figure 2), with correlation coefficients of 0.67. In winter, the hazy weather occurred more frequently and visibility dramatically deteriorated over the Pearl River Delta region [35]. The strong linear correlation between AOT and PM reveals that it is reasonable and feasible to retrieve the spatial distribution of PM from AOT. Factors affecting the accuracy of the models include: (a) AOT are column measurements whereas PM are recorded 5 feet above the ground; (b) the average particle sizes of aerosols increases with increasing relative humidity [36,37]. Therefore, it is concluded that satellite-retrieved aerosol maps provide the possibility and capability of monitoring and characterizing spatio-temporal distribution of the surface PM with a reasonable degree of accuracy.

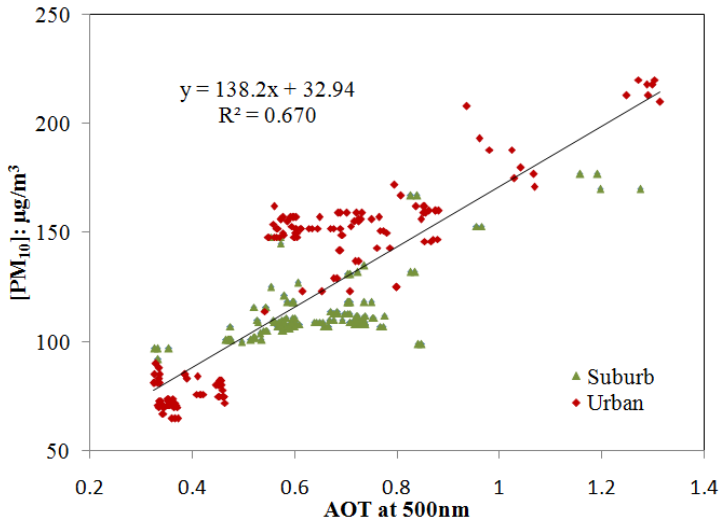

Figure 2. Linear regression between AOT at 500 nm and ground measurements PM_{10}.

4. Retrieval of Atmospheric Particulate Concentrations

A unary linear regression is used to estimate the spatial distribution of particulate matter over the PRD, as expressed in Equation (1):

$$Y = a + bX \quad (1)$$

where Y is the predicted variable, X are the independent variables of the model, a is a constant and b is the coefficient of the variables. In our model, X represents AOT values with high-resolution, and Y is predicted PM concentrations. As Figure 2 shows, PM_{10} and AOT are highly linear-correlated, thus an observed set of values of station-measured PM_{10} concentrations and satellite-derived AOT values at the same place in 2008 could be used to develop the linear model in Figure 3. Then, through the established regression model, the unmeasured PM concentrations in non-station areas can be retrieved from 500 m-resolution aerosol optical thickness, for the satellite-derived AOT maps are spatially continuous, and show values both at station and non-station points.

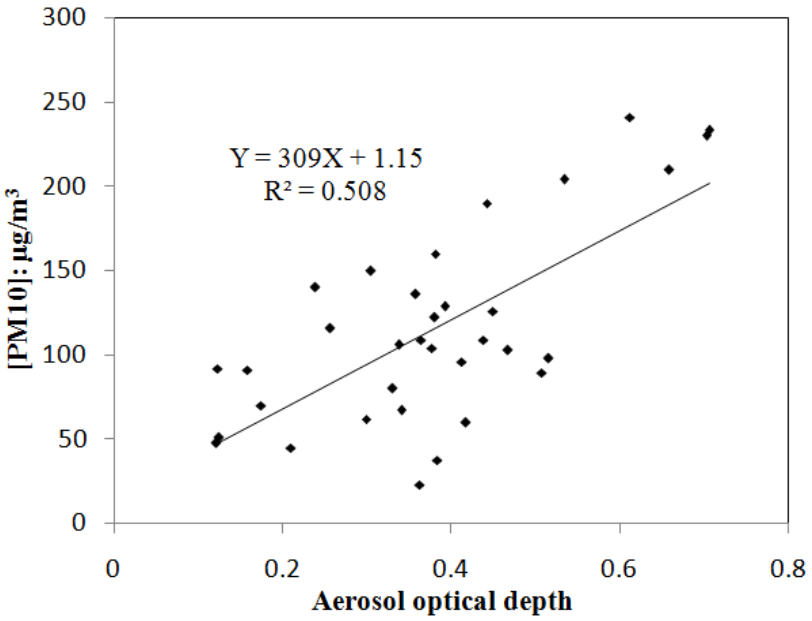

Figure 3. Correlation diagram between average aerosol optical thickness within 500 m radius of the monitoring station and station-measured PM_{10} concentrations.

Retrieval of 500 m-resolution AOT in this study is based on an improved dark dense vegetation (DDV) method, proposed by our previous study [38]. Aerosol products of satellite remote-sensing provide an effective way to study air pollution, but have a conflict between resolution and signal-to-noise ratio (SNR). Our method, on a basis of MOD04-C005 algorithm, hopes to obtain Aerosol Optical Thickness (AOT) with a higher spatial resolution in the case of moderate decreases in SNR [39]. The theory of the method is that in the case of low surface reflectance, the 2.1-μm channel is transparent to most aerosol types so that its apparent reflectance can be considered to be equal to the surface reflectance [40,41]. The relations among the surface reflectance in the blue, red and SWIR band are not a fixed ratio but depend on the scattering angle and $NDVI_{SWIR}$ derived from reflectance at 1.24 and 2.12 μm bands, taking into account the angular variability and surface type, since the Earth's surface is not

Lambertian and some surface types exhibit bidirectional reflectance functions (BRDF). Besides, before AOT retrieval, the MODIS cloud mask products (MOD35_L2) were applied to remove the cloud on MODIS L1B images. For the remaining potentially clear pixels, the selection of dark pixels by discarding brightest 50% and darkest 20% of reflectance at 0.66 μm, also reduce the cloud and surface contamination. Thus, the AOT can be retrieved from the surface reflectance due to the correlation between surface reflection in the blue (0.49 μm), red (0.66 μm), and 2.12 μm bands. Changing the movement pattern of the retrieval window, selecting a more suitable aerosol type, and storing the look-up table as a four-dimensional array, enhance the spatial resolution of AOT considerably relative to MODIS AOT products. The selection of effective dark pixels is conducted in a window of 20 × 20 pixels (10 km × 10 km), and the calculation of the surface reflectance at 0.47 and 0.66 μm are functions of the surface reflectance at 2.13 μm, NDVI and the scattering angle. We also adopted the aerosol type suitable for the study area proposed by Li [21], rather than using the urban or continental aerosols in the 6S model. All of these factors would reduce the errors of AOT retrieval on the bright surfaces, especially in urban areas. The AOT maps by our algorithm are much smoother and show more extensive value ranges with fewer null values. We also validated the retrieval results with ground measurements and 10 km-resolution MODIS AOT products, both showing high precision. We will further validate our retrieval results of aerosol optical thickness in specific seasons and regions once we get ground observations of AOT and PM on a long time scale.

4.1. Retrieval of the Instantaneous Particulate Distribution

Data involved in the retrieval include MODIS L1B data onboard the Terra satellite covering the whole Pearl River Delta, and PM_{10} measurements at 10:00 to 11:00 a.m. at the 15 stations on 2, 3 and 5 January 2008, together with atmospheric boundary height and relative humidity were downloaded from NCEP CFSR on the same days. The MODIS instrument passes the entire Earth twice per day, with Terra in the morning and Aqua in the afternoon, while the PM data at the stations were recorded hourly. To reduce the effects of the difference in temporal resolution on the relationship between PM_{10} and AOT, PM data recorded from 10:00 to 11:00 at the 15 point locations were used to match the Terra data in our study. After deriving the AOT from the MODIS images, the relationship between average AOT values within 500 m radius of the monitoring station and PM_{10} from all sites was established as shown in Figure 3. The accuracy of the relationship is affected by the imperfect match between the spatial-temporal resolutions of AOT-PM data, as the AOT was estimated at about 10:30 a.m. with a spatial resolution of 500 m, and the null values were excluded from the calculation. The PM data, on the other hand were recorded from 10:00 to 11:00 at the 15 point locations. In addition, the relative humidity and atmospheric boundary layer height have impacts on the correlation between column AOT and ground PM_{10} concentrations. The spatial distribution maps of PM_{10} on 2, 3 and 5 January using the linear model in Figure 3 are shown in Figure 4. The difference between the slope values of the models in Figures 2 and 3 is possibly caused by the measuring instruments, and the PM concentrations from ground observations are a little higher than that from the monitoring stations.

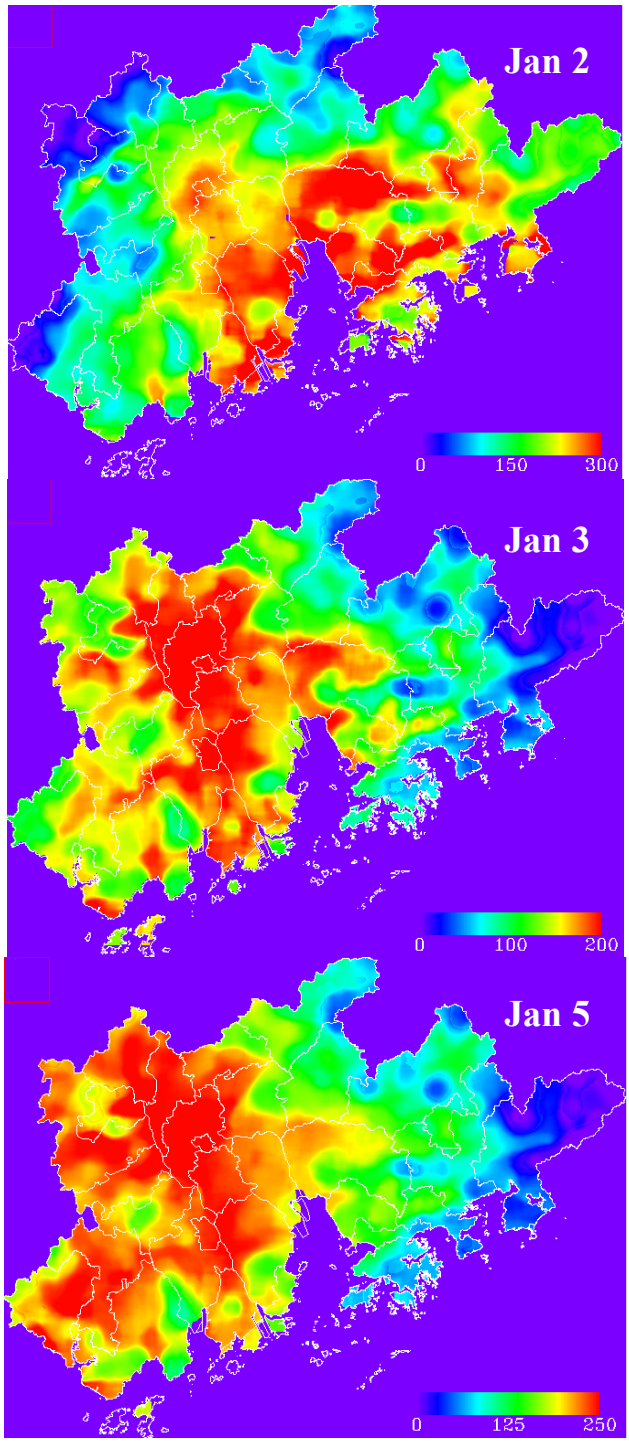

Figure 4. Spatial distribution of PM_{10} derived from 500 m-rsolution AOT in PRD on 2, 3 and 5 January 2008 (unit: $\mu g/m^3$).

Variations in local meteorological conditions and occurrence of multiple aerosol layers play important roles in the relationship between AOT and PM_{10}. To estimate the PM concentrations directly from AOT may be somewhat tenuous, and the vertical distribution of aerosols and the relative humidity, related to atmospheric profiles, ambient condition, the size distributions and chemical compositions of aerosols, are especially important. As AOT reflects the aerosol optical properties of the total column whereas particle matter concentrations are usually recorded at 5 feet above the ground, the relation

between them is greatly influenced by the vertical distribution of aerosols. As we know, AOT is the integral of the extinction coefficient k_a at all altitudes along the vertical orientation, and is expressed as:

$$\tau_\alpha(\lambda) = \int_0^\infty k_a(\lambda, z)dz \tag{2}$$

where $\tau_a(\lambda)$ is the total atmospheric optical thickness, and $k_a(\lambda, z)$ is the extinction coefficient at the altitude of z and the wavelength of λ. Additionally, the vertical distribution of $k_a(\lambda, z)$ could be described as the negative exponent form as:

$$k_a(\lambda, z) \approx k_{a,0}(\lambda)\exp(-z / H_A) \tag{3}$$

where $k_{a,0}(\lambda)$ is the extinction coefficient at the wavelength of λ near the surface, and H_A is the scale height of aerosol, approximately represented by the atmospheric boundary layer height (ABL) [42,43]. Combining Equations (2) and (3), we calculate $\tau_a(\lambda)$ as:

$$\tau_\alpha(\lambda) = k_{a,0}(\lambda)\int_0^\infty \exp(-z / H_A)dz = k_{a,0}(\lambda)\cdot H_A \tag{4}$$

On the other hand, the hygroscopic growth of particles has effects on the refraction and extinction index, as well as other optical properties of aerosols [44]. The correlation between extinction coefficient k_a and PM_{10} is also affected by the chemical components of particles and relative humidity of the air, since the PM_{10} concentrations measured by the instruments are almost the dry mass of the particles with aerodynamic diameter less than 10 μm. Thus, $f(RH)$ is used to define the hygroscopic growing factor as [36,45]:

$$f(RH) = (1 - RH/100)^{-g} \tag{5}$$

where g is an empirical fie coefficient and set as 1 in our study. The dry $k_{a,0}(\lambda)$ is obtained from

$$k_{\alpha,DRY}(\lambda) = k_{a,0}(\lambda) / f(RH) \tag{6}$$

Hence, we could calculate the aerosol extinction coefficient in the dry air near the surface $k_{a,DRY}(\lambda)$ from Equation (1) to Equation (5), and express it as

$$k_{\alpha,DRY}(\lambda) = \tau_a(\lambda) / [H_A \cdot (1 - RH/100)^{-g})] \tag{7}$$

Wang *et al.* [24] once described the relationship between k_a and PM concentration on the basis of the Mie theory as

$$k_\alpha = \frac{3\langle Q_{ext}\rangle}{4r_{eff}\rho} PM_x \tag{8}$$

where Q_{ext} is the size distribution integrated extinction efficiency, r_{eff} is the effective radius, being approximately constant, and PMx is the mass concentration of PM. Therefore, it is possible to develop a linear correlation between $k_{a,DRY}(\lambda)$ and PM_{10} concentrations, like

$$PM_{10} = a \times k_{a,DRY} + b \tag{9}$$

Furthermore, the vertical and relative humidity corrections on AOT could enhance the relationship and increase the robustness of the estimate.

Spatial distributions of ABL height and relative humidity on 2 and 3 January are displayed in Figure 5. The comparison of measurements at the weather stations and forecast of relative humidity is shown in Figure 6, with a correlation coefficient of 0.816. The deviation of the correlation is caused by the different temporal resolutions of these two datasets. Data from NCEP CFSR was at 6-hourly intervals while the station observations are hourly averaged.

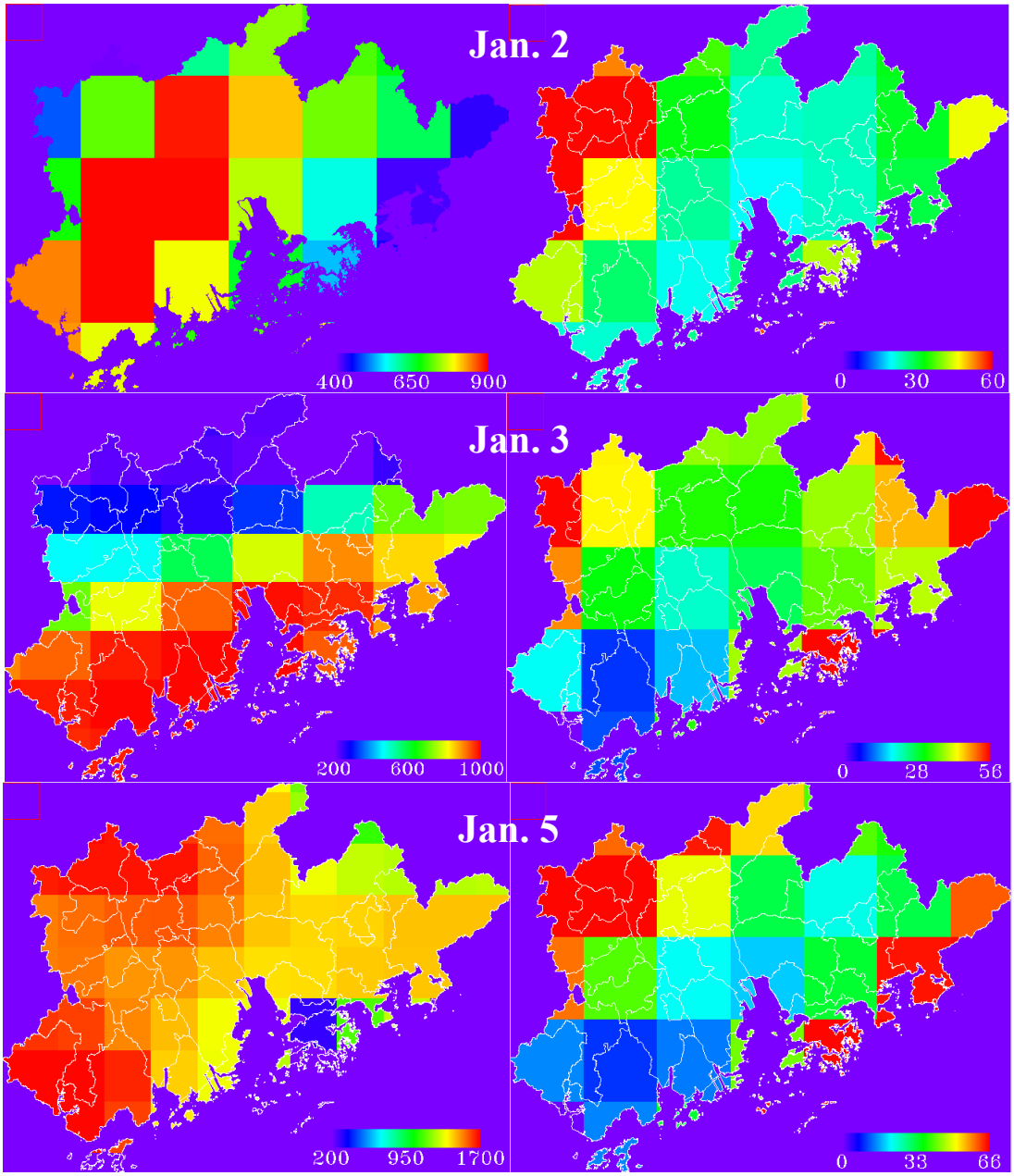

Figure 5. Spatial distribution of atmospheric boundary layer (ABL) height (unit: meter) on the left and relative humidity (unit: %) on the right in PRD at 6:00 UTC on 2, 3 and 5 January 2008, provided by NCEP CFSR, with a resolution of 0.5 degree.

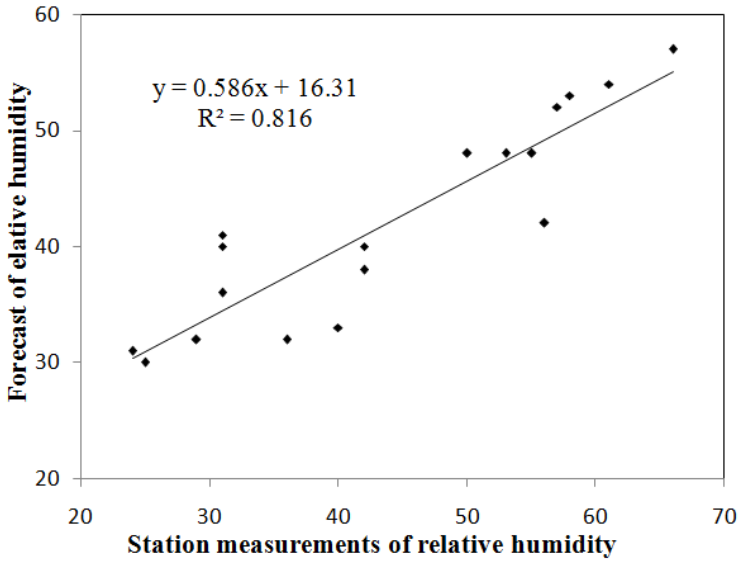

Figure 6. The scatter plot of measurements at the weather stations and forecast of relative humidity from NCEP CFSR.

ABL height and relative humidity data at 6:00 UTC (14:00 pm local time), which are the closest datasets to the overpassing time of satellite, were applied to the vertical and humidity correction on MODIS Terra images to reduce the errors from temporal scale. The correlation between average corrected $k_{\mathrm{AOT,DRY}}(\lambda)$ and PM_{10} is shown in Figure 7. Comparison between Figures 3 and 7 indicates that the correlation ($R^2 = 0.55$) is slightly higher after this correction but not significant, mainly because of the low spatial resolution of meteorological data. The final retrieved PM_{10} images over the Pearl River Delta on 2, 3 and 5 January are displayed in Figure 8.

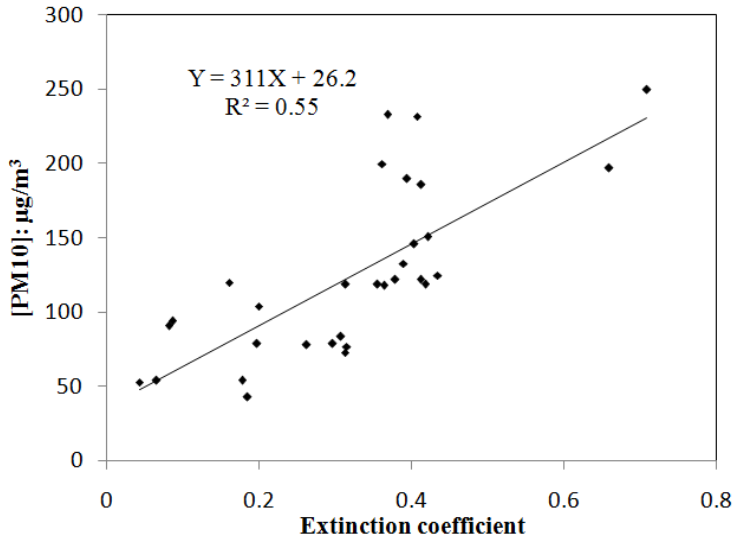

Figure 7. Correlation between extinction coefficient and surface-level PM_{10} after vertical and humidity correction using meteorologic data form NCEP CFSR.

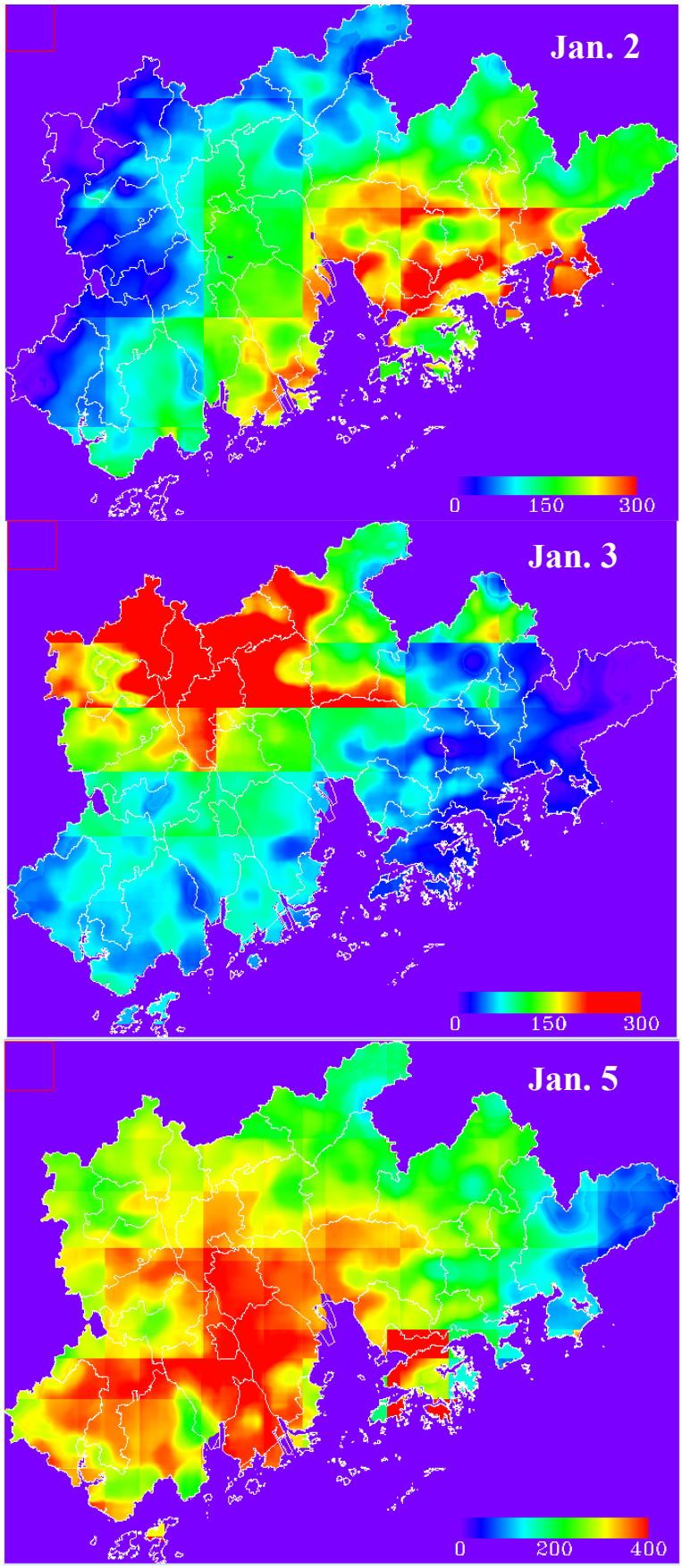

Figure 8. Spatial distribution of PM_{10} in PRD on 2, 3 and 5 January 2008 after vertical and humidity correction (unit: $\mu g/m^3$).

The coarse spatial resolution of meteorological data leads to apparent grids in the images in Figure 8. We therefore averaged the values of ABL height and relative humidity from NECP CFSR over the PRD to smooth and refine the maps. To do so, we took H_A and RH in Equation (2) to be single valued rather than maps with 0.5° resolution. The relationship between corrected AOT and PM_{10} is shown in Figure 9 with a coefficient of 0.531. It indicates that the correlation can be enhanced by vertical and humidity corrections, but the degree of improvement depends on the accuracy of the meteorological data. The retrieved PM_{10} images over the Pearl River Delta on 2, 3 and 5 January are displayed in Figure 10.

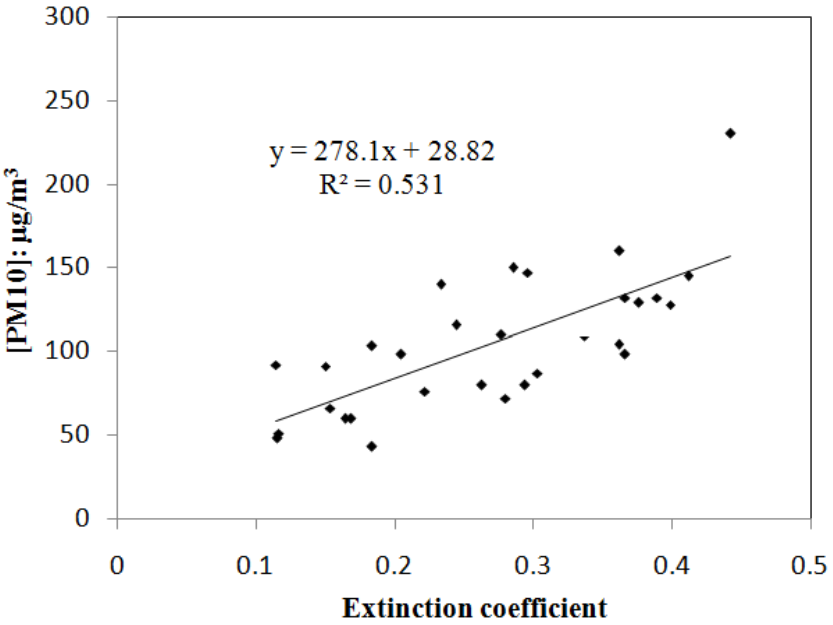

Figure 9. Correlation between extinction coefficient corrected by average value of atmospheric boundary layer height and relative humidity, and the surface-level PM_{10}.

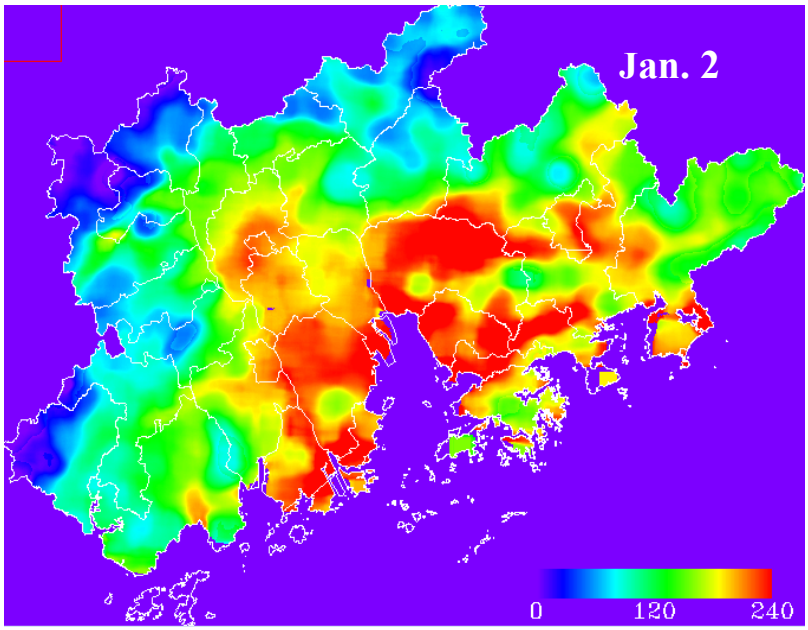

Figure 10. *Cont.*

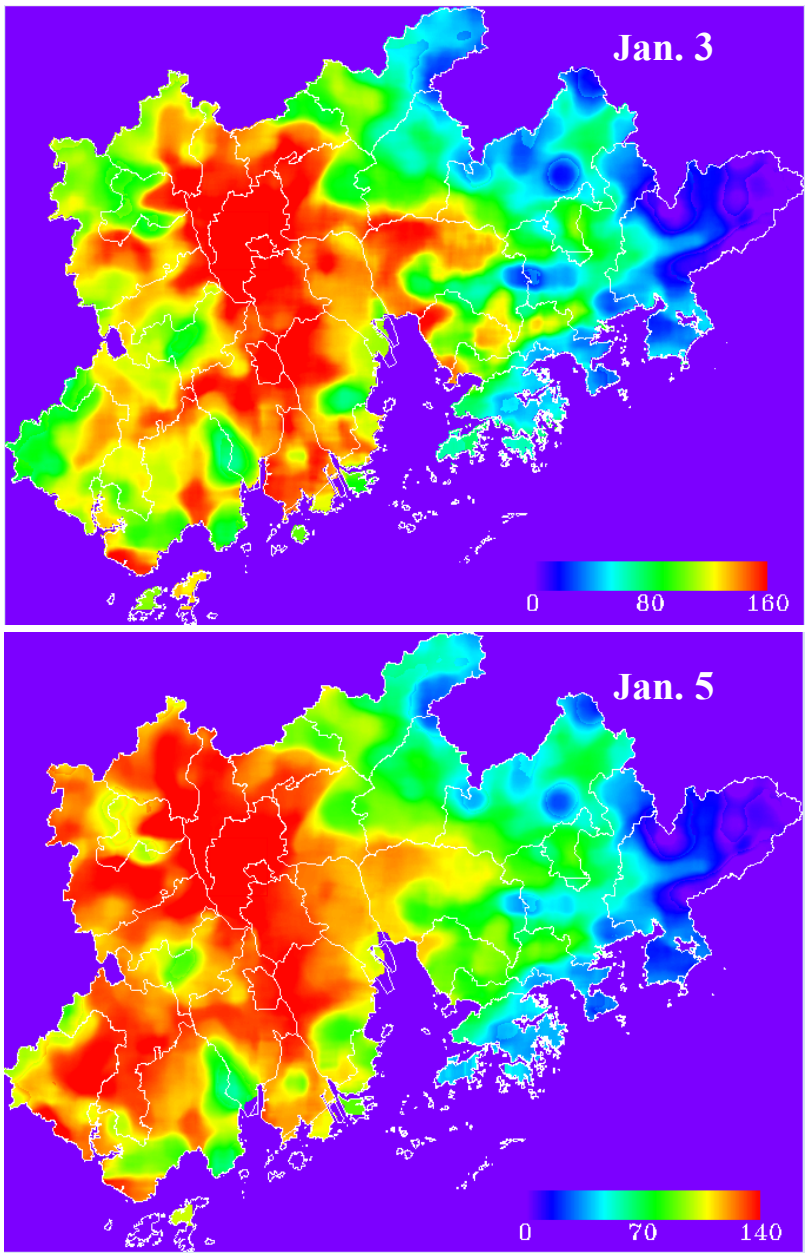

Figure 10. Spatial distribution of derived PM_{10} in PRD on 2, 3 and 5 January 2008 after correction (unit: $\mu g/m^3$).

4.2. Retrieval of Yearly Average PM_{10} Distributions

We used all cloud-free MODIS data in 2008 to derive the corresponding AOT using the dark dense vegetation method. Averaging the results leads to an estimate of the yearly aerosol optical thickness over the PRD Figure 11. However, in summer the common occurrence of clouds makes AOT rarely observable, thus only a few MODIS images were studied. The average results would be a little lower since AOT values in summer are higher than these in winter [46]. Additionally we estimated the PM concentrations in non-site areas from our regression model. According to the station measurements provided by Guangdong Environmental Protection Bureau, the days of PM_{10} exceeding the standard threshold 150 $\mu g/m^3$ in 2008 were 5 in Tianhu, 11 in Luhu Park, 46 in Xiapu, 20 in Chenzhong, 37 in Hangang School, 63 in Huijingcheng, 1 in Jinguowan, 27 in Jinjuzui, 43 in Wanqinsha, 23 in Donghu, 5

in Liyuan, 35 in Zimaling Park, 2 in Tamen, 1 in Quanwan and 0 in Tangjia, respectively. Linear regression of these data is shown in Figure 12 with a correlation coefficient of 0.582. The slope coefficient in the linear regression model of yearly average AOT and PM_{10} is relatively low, probably because of the average calculation on AOT and fewer sample points. The correlation between yearly mean AOT and observed PM_{10} is slightly higher than that between the instantaneous values, mainly because averaging tends to eliminate outliers. The instantaneous AOT is influenced by many factors that show frequent fluctuations, such as temperature, monsoon, and precipitation, as well as human activities, such as fossil fuel burning. Retrieved AOT maps cannot reflect the true air quality when there appears to be a low or high value anomaly of these factors. Occurrence of clouds also makes aerosols sometimes rarely observable, accompanied by null values of AOT. Outliers and missing data may introduce bias or affect the representativeness of the results. The yearly average AOT can remove the occasional effects and eliminate the outliers of AOT by replacing them with the average values of the pixel. Thus, the larger the time scales, the higher the correlation between aerosol optical thickness and PM_{10} concentration. The yearly average PM_{10} is then retrieved through the regression equation (Figure 13).

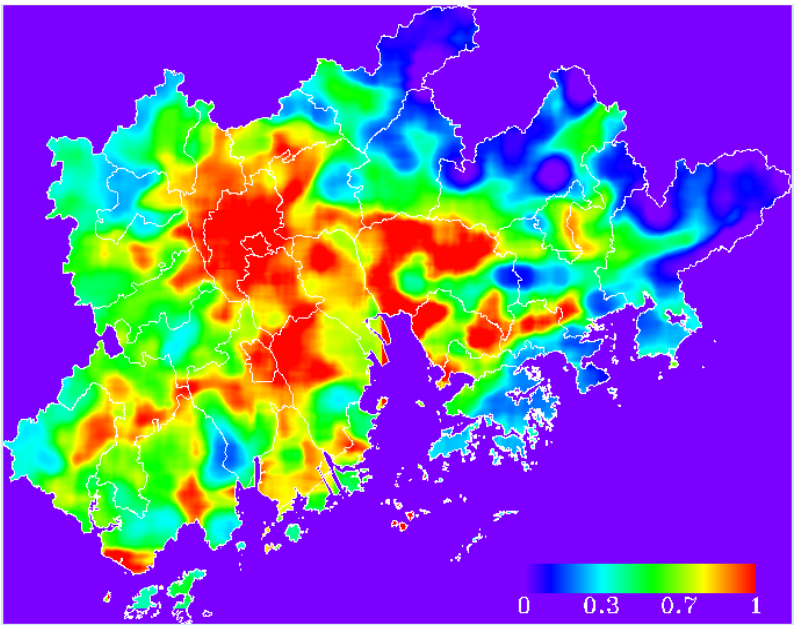

Figure 11. A 500 m-resolution yearly average aerosol optical thickness in 2008 over the Pearl River Delta region retrieved from all cloud-free MODIS L1B data by using an improved Dark Dense Vegetation method.

Table 5 lists the yearly average values of AOT, measured PM_{10} and regressive PM_{10} of the 15 monitoring stations in PRD, 2008. The predicted PM_{10} was derived from the model shown in Figure 12, by putting in the yearly average AOT values at each monitoring station. The deviations between the actually-measured and predicted PM_{10} concentrations were calculated to indicate the stability of the model. The root mean square error (RMSE) between station measured PM_{10} and the predicted PM_{10} was calculated from the deviations to be ±10 $\mu g/m^3$, indicative of the reliability of the retrieved results while the relative errors of the predicted results are from 1.75% to 27.12%, showing the limitations of the applicability of the model. Air quality at most sites is poor according to the standards of both yearly average PM_{10} (70 $\mu g/m^3$) laid down in the ambient air quality standards. Figure 13 show that areas with

the worst air pollution are located in Foshan city, at the border of Shunde and Zhongshan, west of Gongguan, and northwest of Shenzhen.

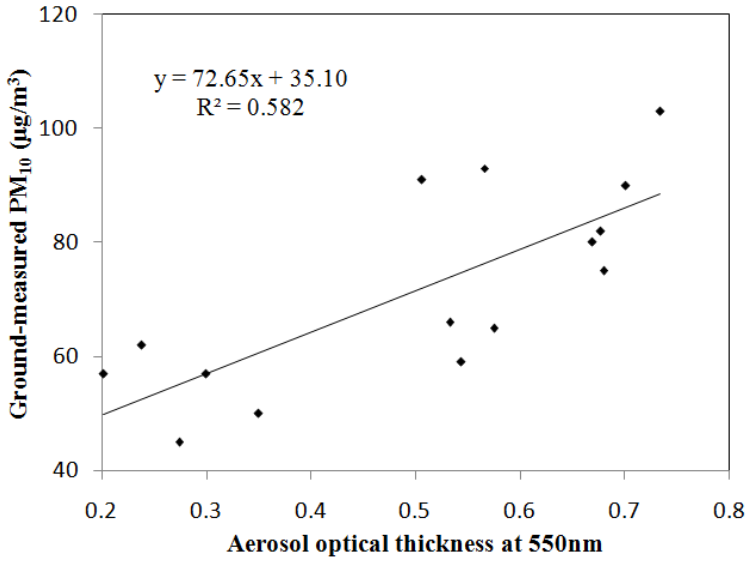

Figure 12. Regression analysis between the yearly averaged retrieved AOT and ground-measured PM_{10} of the 15 monitoring stations in the PRD, 2008.

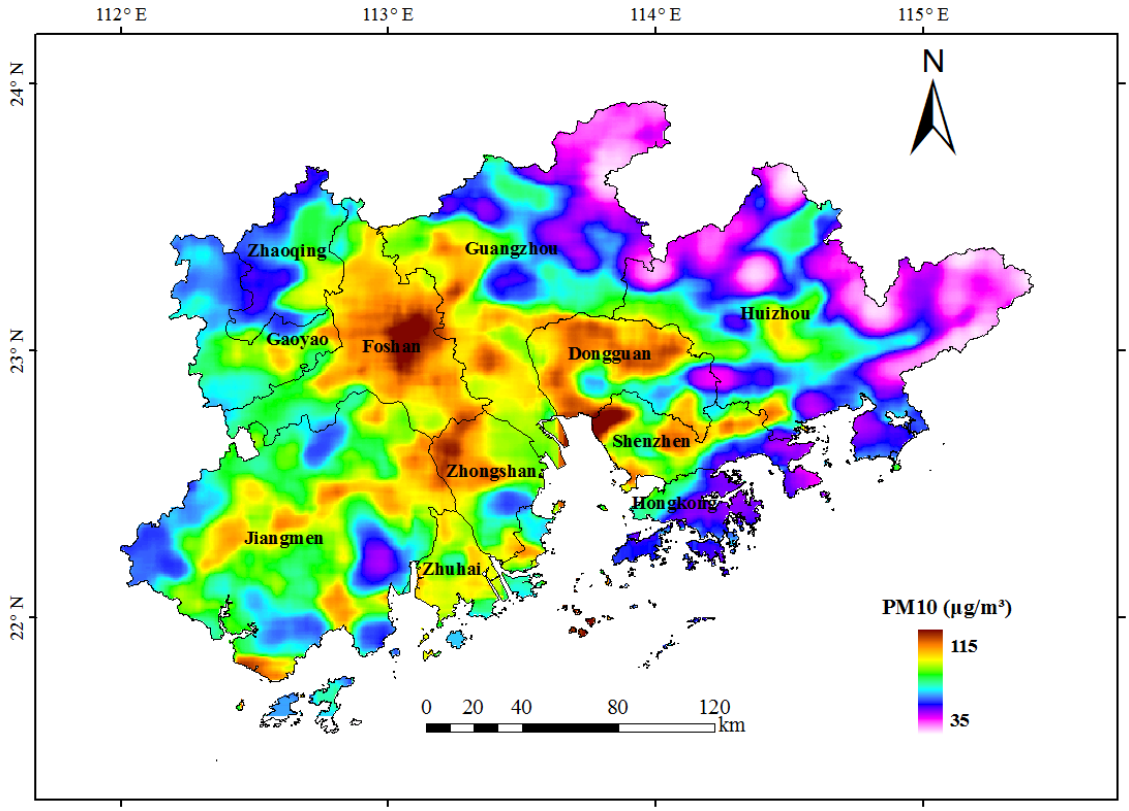

Figure 13. Spatial distribution of retrieved yearly average PM_{10} concentrations in the PRD, 2008 (unit: $\mu g/m^3$).

Table 5. Yearly average values of AOT, measured PM_{10} and Predicted PM_{10} of the 15 monitoring stations in the PRD, 2008.

Sites	AOT	Measured PM_{10} ($\mu g/m^3$)	Predicted PM_{10} ($\mu g/m^3$)	Deviation ($\mu g/m^3$)	Relative Errors (%)
Tianhu	0.238	62	54	−8	−12.90
Luhu Park	0.575	65	77	12	18.46
Haogang school	0.701	90	86	−4	−4.44
Xiapu	0.506	91	72	−19	−20.88
Jinguowan	0.274	45	56	11	24.44
Liyuan	0.544	59	75	16	27.12
Tamen	0.3	57	58	1	1.75
Quanwan	0.202	57	51	−6	−10.53
Tangjia	0.35	50	61	11	22.00
Zimaling Park	0.677	82	84	2	2.44
Wanqinsha	0.566	93	76	−17	−18.28
Donghu	0.68	75	84	9	12.00
Jinjuzui	0.669	80	84	4	5.00
Huijingcheng	0.734	103	88	−15	−14.56
Chengzhong	0.533	66	74	−8	−12.12

5. Conclusions

Analysis on the size distribution of particles indicates that most of the atmospheric particulate matters in Pearl River Delta region are inhaled particles of small sizes. Simultaneous observations of AOT and PM_{10} are proved to be strongly correlated; R^2 being 0.670. It forms the basis for successful linear regression between AOT and PM.

A linear regression ($R^2 = 0.51$) is carried out using MODIS-derived 500 m-resolution aerosol optical thickness and PM_{10} concentration from monitoring stations on 2, 3 and 5 January 2008. However, the relationship between AOT and PM over PRD is not necessarily suitable for other regions because of regional variations in aerosols type, sources, and air pollution affecting the relationship between AOT and PM. In addition the relationship may vary over time, for seasonal differences in climate would affect the formation and movement of atmospheric particles. The model in our study successfully demonstrates the possibility and feasibility of retrieval particulate matters from satellite-derived AOT, especially high-resolution AOT maps, which makes air quality monitoring in smaller regions more reliable. The correlation between AOT and PM_{10} also increased a little after vertical and relative humidity correction. Our further work aims at using more accurate meteorological data to increase retrieval accuracy for air pollution assessment.

Retrieval of atmospheric particulate concentrations shows that yearly mean AOT and observed PM_{10} correlate better than instantaneous values, and the root mean square error (RMSE) of our predictive model was 0.01.The yearly average particle matter concentration in 2008 shows the four most polluted regions to be: Foshan city, the border between Shunde and Zhongshan, the area to the west of Dongguan, and the northwest of Shenzhen.

However, there still exist some uncertainties in the linear model. The relationship between AOT and PM varies with time and region, and the chemical reactions in the air are more complicated than the

linear regression models reflect [47]. Assimilating the satellite products and meteorological data into numerical models could be a good way to retrieve the spatial distributions of PM. Also, the relation between AOT and PM are influenced by the lack of accurate information on particle composition, size distribution and vertical profile. It is also affected by the accuracy and spatio-temporal resolution of the input data. The variations of water vapor could lead to the swelling or condensation of particles, and consequently the change of the microstructure and composition of the particles, which affects the relationship between AOT and PM. Vertical profile of aerosols could also introduce errors in the relationship, because of the significant contribution of aerosols above the boundary layer to extinction, especially when weak atmospheric convection happens [48]. Therefore, information on the aerosol vertical profiles from ground-based lidars and space-borne lidars, such as the Cloud-Aerosol Lidar and Infrared Pathfinder Satellite Observations (CALIPSO), could be applied into the retrieval of PM from satellite data. The accuracy of the input data, like the satellite-derived AOT, the instruments for ground measurements and the meteorological data for corrections, would also affect the linear model between AOT and PM. Furthermore, the satellite images covering the local region are obtained twice a day, and have a relatively coarse spatial resolution, while the station data are measured on the ground all day. The imperfect match of spatio-temporal resolution between satellite data and surface observations brings errors to the model. The seasonal variation of the relationship is another issue that should be taken into account. The seasonal difference in the meteorological conditions, such as temperature, precipitation and relative humidity, and human activities could result in the change of the relationship.

Acknowledgments

China National Key Technology R&D Program (2012BAH32B03), China National 863 Program (2006AA06A306), China NSFC (41401485) and Guangdong NSF (S2013010014097) are acknowledged for financial supports. We also thank the NASA Earth System for the MODIS products and Guangdong Environmental Protection Bureau for the station monitoring data. Bernard de Jong of Utrecht University and Z. Zhou of Lancaster University are thanked for comments and corrections. This is contribution No. SKLOG2013A01 from SKLOG and No. IS-2088 from GIGCAS.

Author Contributions

The study was completed by all authors. Lili Li, Jingxue Yang and Yunpeng Wang conceived and designed the experiments; Lili Li and Jingxue Yang performed the experiments and analyzed the data; Lili Li wrote the paper; Yunpeng Wang checked the experimental results and finalized the paper.

Conflicts of Interest

The authors declare no conflict of interest.

References

1. King, M.D.; Kaufman, Y.J.; Tanré, D.; Nakajima, T. Remote sensing of tropospheric aerosols from space: Past, present and future. *Bull. Am. Meteorol. Soc.* **1999**, *80*, 2229–2259.

2. Kaufman, Y.J.; Tanré, D.; Boucher, O. A satellite view of aerosols in the climate system. *Nature* **2002**, *419*, 215–223.
3. Dockery, D.W.; Pope, C.A.; Xu, X.P.; Spengler, J.D.; Ware, J.H.; Fay, M.E.; Ferris, B.G., Jr.; Speizer, F.E. An association between air pollution and mortality in six U.S. cities. *N. Engl. J. Med.* **1993**, *329*, 1753–1759.
4. Schwartz, J.; Dockery, D.W.; Neas, L.M. Is daily mortality associated specifically with fine particles? *J. Air Waste Manag. Assoc.* **1996**, *46*, 927–939.
5. Pope, C.A., III. Review: Epidemiological basis for particulate air pollution health standards. *Aerosol Sci. Technol.* **2000**, *32*, 4–14.
6. Samet, J.M.; Dominici, F.; Curriero, F.C.; Coursac, I.; Zeger, S.L. Fine particulate air pollution and mortality in 20 U.S. cities, 1987–1994. *N. Engl. J. Med.* **2000**, *343*, 1742–1749.
7. Wallace, L. Correlations of personal exposure to particles with outdoor air measurements: A review of recent studies. *Aerosol Sci. Technol.* **2000**, *32*, 15–25.
8. Husar, R.B.; Tratt, D.M.; Schichtel, B.A.; Falke, S.R.; Li, F.; Jaffe, D.; Gassó, S.; Gill, T.; Malm, W.C. Asian dust events of April 1998. *J. Geophys. Res.: Atmos.* **2001**, *106*, 18317–18330.
9. Hutchison, K.D. Applications of MODIS satellite data and products for monitoring air quality in the state of Texas. *Atmos. Environ.* **2003**, *37*, 2403–2412.
10. Wang, J.; Christopher, S.A.; Reid, J.S.; Maring, H.; Savoie, D.; Holben, B.N.; Livingston, J.M.; Russell, P.B.; Yang, S.-K. GOES 8 retrieval of dust aerosol optical thickness over the Atlantic Ocean during PRIDE. *J. Geophys. Res.: Atmos.* **2003**, *108*, doi:10.1029/2002JD002494.
11. Engel-Cox, J.A.; Holloman, C.H.; Coutant, B.W.; Hoff, R.M. Qualitative and quantitative evaluation of MODIS satellite sensor data for regional and urban scale air quality. *Atmos. Environ.* **2004**, *38*, 2495–2509.
12. Engel-Cox, J.A.; Young, G.S.; Hoff, R.M. Application of satellite remote-sensing data for source analysis of find particulate matter transport events. *J. Air Waste Manag. Assoc.* **2005**, *55*, 1389–1397.
13. Kacenelenbogen, M.; Léon, J.F.; Chiapello, I.; Tanré, D. Characterisation of aerosol pollution events in France using ground-based and POLDER-2 satellite data. *Atmos. Chem. Phys.* **2006**, *6*, 4843–4849.
14. Schaap, M.; Apituley, A.; Timmermans, R.M.A.; Koelemeijer, R.B.A.; de Leeuw, G. Exploring the relation between aerosol optical depth and PM2.5 at Cabauw, The Netherlands. *Atmos. Chem. Phys.* **2009**, *9*, 909–925.
15. Malm, W.C.; Sisler, J.F.; Huffman, D.; Eldred, R.A.; Cahill, T.A. Spatial and seasonal trends in particle concentration and optical extinction in the United States. *J. Geophys. Res.* **1994**, *99*, 1347–1370.
16. Chow, J.C.; Watson, J.G.; Lowenthal, D.H.; Richards, L.W. Comparability between $PM_{2.5}$ and particle light scattering measurements. *Environ. Monit. Assess.* **2002**, *79*, 29–45.
17. Wang, J.; Christopher, S.A. Intercomparison between satellite-derived aerosol optical thickness and $PM_{2.5}$ mass: Implications for air quality studies. *Geophys. Res. Lett.* **2003**, *30*, doi:10.1029/2003GL018174.

18. Chu, D.A.; Kaufman, Y.J.; Zibordi, G.; Chern, J.D.; Mao, J.T.; Li, C.C.; Holben, B.N. Global monitoring of air pollution over land from the Earth Observing System-Terra Moderate Resolution Imaging Spectroradiometer (MODIS). *J. Geophys. Res.: Atmos.* **2003**, doi:10.1029/2002JD003179.
19. Engel-Cox, J.A.; Hoff, R.M.; Rogers, R.; Dimmick, F.; Rush, A.C.; Szykman, J.J.; Al-Saadi, J.; Chu, D.A.; Zell, E.R. Integrating lidar and satellite optical depth with ambient monitoring for 3-D dimensional particulate characterisation. *Atmos. Environ.* **2006**, *40*, 8056–8067.
20. Gupta, P.; Christopher, S.A.; Wang, J.; Gehrig, R.; Lee, Y.C.; Kumar, N. Satellite remote sensing of particulate matter and air quality assessment over global cities. *Atmos. Environ*. **2006**, *40*, 5880–5892.
21. Li, C.C.; Lau, A.K.-H.; Mao, J.T.; Chu, D.A. Retrieval, validation and application of the 1-km aerosol optical depth from MODIS measurement over Hong Kong. *IEEE Trans. Geosci. Remote Sens.* **2005**, *43*, 2650−2658.
22. Zheng J.Y.; Che W.W.; Zheng Z.Y.; Chen L.F.; Zhong L.J. Analysis of spatial and temporal varialility of PM10 concentrations using MODIS aerosol optical thickness in the Pearl River Delta region, China. *Aerosol Air Qual. Res.* **2013**, *13*, 862–876.
23. Guo, J.P.; Zhang, X.Y.; Che, H.Z.; Gong, S.L.; An, X.; Cao, C.X.; Li, X.W. Correlation between PM concentrations and aerosol optical depth in eastern China. *Atmos. Environ*. **2009**, *43*, 5876–5886.
24. Wang, Z.F.; Chen, L.F.; Tao, J.H.; Zhang, Y.; Su, L. Satellite-based estimation of regional particulate matter (PM) in Beijing using vertical-and-RH correcting method. *Remote Sens. Environ.* **2010**, *114*, 50–63.
25. You, W.; Zang, Z.; Pan, X.; Zhang, L.; Chen, D. Estimating PM2. 5 in Xi'an, China using aerosol optical depth: A comparison between the MODIS and MISR retrieval models. *Sci. Total Environ.* **2015**, *505*, 1156–1165.
26. Huang, D.S.; Xu, J.H.; Zhang, S.Q. Valuing the health risks of particulate air pollution in the Pearl River Delta, China. *Environ. Sci. Policy* **2012**, *15*, 38–47.
27. Wu, D.; Deng, X.J.; Bi, X.Y.; Li, F.; Tan, H.B.; Liao, G.L. Study on the visibility reduction caused by atmospheric haze in Guangzhou area. *J. Trop. Meteorol.* **2007**, *23*, 1–6.
28. Deng, X.J.; Tie, X.X.; Wu, D.; Zhou, X.J.; Bi, X.Y.; Tan, H.B.; Li, F.; Jiang, C.L. Long-term trend of visibility and its characterizations in the Pearl River Delta (PRD) region, China. *Atmos. Environ.* **2008**, *42*, 1424–1435.
29. Huang, J.; Wu, D.; Huang, M.H.; Li, F.; Bi, X.Y.; Tan, H.B.; Deng, X.J. Visibility variations in the Pearl River Delta of China during the Period of 1954–2004. *J. Appl. Meteorol. Sci.* **2008**, *19*, 61–70.
30. Xie, P.; Liu, X. Y, Liu, Z. R, Li, T.T.; Zhong, L.J.; Xiang, Y.R. Human health impact of exposure to airborne particulate matter in Pearl River Delta, China. *Water Air Soil Pollut.* **2011**, *215*, 349–363.
31. Watson, J.G.; Chow, J.C.; Chen, L.; Wang, X.L.; Merrifield, T.M.; Fine, P.M.; Barker, K. Measurement system evaluation for upwind/downwind sampling of fugitive dust emissions. *Aerosol Air Qual. Res.* **2011**, *11*, 331–350.
32. The National Centers for Environmental Prediction (NCEP) Climate Forecast System Reanalysis (CFSR) 6-hourly Products, January 1979 to December 2010. Available online: http://dx.doi.org/10.5065/D69K487J (accessed on 5 January 2008).

33. Saha, S.; Suranjana, M.; Pan, H.L.; Wu, X.G.; Wang, J.D.; Sudhir, N.; Patrick, T.; Glenn, R.; Mitch, G. The NCEP Climate Forecast System Reanalysis. *Am. Meteorol. Soc.* **2010**, *91*, 1015–1057.
34. Wu, D.; Bi, X.Y.; Deng, X.J.; Li, F.; Tan, H.B.; Liao, G.L.; Huang, J. Effect of atmospheric haze on the deterioration of visibility over the Pearl River Delta. *Acta Meteorol. Sin.* **2006**, *64*, 510–517.
35. Wu, D.; Lau, A.K.-H. Leung, Y.K. Hazy weather formation and visibility deterioration resulted from fine particulate (PM2.5) pollutions in Guangdong and Hong Kong. *Acta Sci. Circumst.* **2012**, *32*, 2660–2669.
36. Kotchenruther, R.B.A.; Hobbs, P.V.; Hegg, D.A. Humidification factors for atmospheric aerosols off the mid-Atlantic coast of the United States. *J. Geophys. Res.: Atmos.* **1999**, *104*, 2239–2251.
37. Li, C.C.; Mao, J.T.; Liu, Q.H.; Yuan, Z.B.; Wang, M.H.; Liu, X.Y. Application of MODIS aerosol product in the study of air pollution in Beijing. *Sci. China Series D Earth Sci.* **2005**, *35*, 177–186.
38. Li, L.L.; Yang, J.X.; Wang, Y.P. An improved dark object method to retrieve 500 m-resolution AOT (Aerosol Optical Thickness) image from MODIS data: A case study in the Pearl River Delta area, China. *ISPRS J. Photogramm. Remote Sens.* **2014**, *89*, 1–12.
39. Levy, R.C.; Remer, L.A.; Mattoo, S.; Vermote, E.F.; Kaufman, Y.J. Second-generation operational algorithm: Retrieval of aerosol properties over land from inversion of Moderate Resolution Imaging Spectroradiometer spectral reflectance. *J. Geophys. Res.: Atmos.* **2007**, *112*, doi:10.1029/2006JD007811.
40. Kaufman, Y.J.; Tanré, D.; Remer, L.A.; Vermote, E.F.; Chu, A.; Holben, B.N. Operational remote sensing of tropospheric aerosol over land from EOS moderate resolution imaging spectroradiometer. *J. Geophys. Res.: Atmos.* **1997**, *102*, 17051–17067.
41. Kaufman, Y.J.; Wald, A.E.; Remer, L.A.; Gao, B.C.; Li, R.R.; Flynn, L.; The MODIS 2.1-μm channel-correlation with visible reflectance for use in remote sensing of aerosol. *IEEE Trans. Geosci. Remote Sens.* **1997**, *35*, 1286–1298.
42. Koelemeijer, R.B.; Homan, C.D.; Matthijsen, J. Comparison of spatial and temporal variations of aerosol optical thickness and particulate matter over Europe. *Atmos. Environ.* **2006**, *40*, 5304–5315.
43. Liu, Y.; Sarnat, J.A.; Kilaru, V.; Jacob, D.J.; Koutrakis, P. Estimating ground-level PM2.5 in the eastern United States using satellite remote sensing. *Environ. Sci. Technol.* **2005**, *39*, 3269−3278.
44. Liu, X.G.; Cheng, Y.F.; Zhang, Y.H.; Jung, J.S.; Sugimoto, N.; Chang, S.Y.; Kim, Y.J.; Fan, S.J.; Zeng, L.M. Influences of relative humidity and particle chemical composition on aerosol scattering properties during the 2006 PRD. *Atmos. Environ*. **2008**, *42*, 1525–1536.
45. Im, J.S.; Saxena, V.K.; Wenny, B.N. An assessment of hygroscopic growth factors for aerosols in the surface boundary layer for computing direct radiative forcing. *J. Geophys. Res.: Atmos.* **2001**, *106*, 20213–20224.
46. Li, L.L.; Wang, Y.P. What drives the aerosol distribution in Guangdong-the most developed province in Southern China? *Sci. Rep.* **2014**, *4*, doi:10.1038/srep05972.
47. Duncan, B.N.; Prados, A.I.; Lamsal, L.N.; Liu, Y.; Streets, D.G.; Gupta, P.; Hilsenrath, E.; Ziemba, L.D. Satellite data of atmospheric pollution for US air quality applications: Examples of applications, summary of data end-user resources, answers to FAQs, and common mistakes to avoid. *Atmos. Environ.* **2014**, *94*, 647–662.

48. Bergin, M.H.; Schwartz, S.E.; Halthore, R.N.; Ogren, J.A.; Hlavka, D.L. Comparison of aerosol optical depth inferred from surface measurements with that determined by Sun photometry for cloud-free conditions at a continental U.S. site. *J. Geophys. Res.* **2000**, *105*, 6807–6816.